Composites Part B 238 (2022) 109920

Contents lists available at ScienceDirect

Composites Part B

journal homepage: www.elsevier.com/locate/compositesb

# Electrospun biodegradable nanofibers loaded with epigallocatechin gallate for guided bone regeneration

Liang Song [a,b,1], Xianrui Xie [c,1], Cuiting Lv [d,1], Atta ur Rehman Khan [e], Yang Sun [a], Ruixue Li [a], Juan Yao [a], Mohamed EL-Newehy [f], Hany EL-Hamshary [f], Yosry Morsi [g], Xiumei Mo [c,**], Youcheng Yu [a,*]

[a] Department of Stomatology, Zhongshan Hospital of Fudan University, 180 Fenglin Road, Shanghai, 200032, China
[b] Department of Stomatology, Shanghai Fifth People's Hospital, Fudan University, 801 Heqing Road, Shanghai, 200240, China
[c] State Key Laboratory for Modification of Chemical Fibers and Polymer Materials, Shanghai Engineering Research Center of Nano-Biomaterials and Regenerative Medicine, College of Chemistry, Chemical Engineering and Biotechnology, Donghua University, 2999 North Renmin Road, Shanghai, 201620, China
[d] Central Laboratory, Shanghai Fifth People's Hospital, Fudan University, 801 Heqing Road, Shanghai, 200240, China
[e] Department of Biotechnology, The University of Azad Jammu & Kashmir, Muzaffarabad, 13100, Pakistan
[f] Department of Chemistry, College of Science, King Saud University, P.O. Box 2455, Riyadh, 11451, Saudi Arabia
[g] Faculty of Engineering and Industrial Sciences, Swinburne University of Technology, Boroondara, VIC, 3122, Australia

ARTICLE INFO

*Keywords:*
Guided bone regeneration
Polymer (textile) fibre
Cure behavior
Micro-mechanics
Mechanical testing

ABSTRACT

Guided bone regeneration through biomaterial-based formulations can prevent soft tissue migration into the bone defect area through a barrier membrane. However, bone regeneration requires bioactive external interference. Here, we report a biodegradable electrospun poly-L-lactic acid/gelatin-based nanofibrous membrane encapsulating epigallocatechin gallate (EGCG) within the core, with a smooth profile, desirable physicochemical properties, biocompatibility, antibacterial effects, sufficient osteoinductive capability, and sustained EGCG release over one week. 70% of the defect area was repaired with the help of the EGCG-loaded membrane, approximately 1.5-fold improvement over the control group in 8 weeks. In conclusion, these membranes are promising candidates for guided bone regeneration.

## 1. Introduction

Bone loss or dysfunction resulting from trauma, injury, disease, or aging poses a significant threat to health and economics. Bone healing quality is adversely affected by multiple factors, including oxidative stress, inflammation, and fat deposition, which may inhibit the inductive signals required for osteoblastogenesis and progenitor cell recruitment [1–3]. In this regard, therapeutic biomaterials capable of guiding and signaling for efficient bone regeneration can certainly provide relief to the patient [4].

Guided bone regeneration (GBR) is considered the most desirable strategy for treating periodontal defects. It employs a barrier membrane capable of preventing fibroblast and epithelial cell influx, blocking the sites for periodontal tissue reconstruction into defect areas [5]. Although GBR-based therapeutic approaches have played a significant role in bone tissue regeneration, their lack of bioactivity presents several disadvantages [6]. In other words, these scaffolds usually act as physical barriers but lack regenerative signals and antibacterial potential [7]. Moreover, conventional membranes are composed of non-biodegradable materials, accompanied by the risk of secondary damage to newly formed tissue, usually requiring surgery for their removal from the defect area [8]. Therefore, a new therapeutic strategy in the form of a biodegradable active membrane capable of serving as both a barrier membrane and carrier containing the optimal bioactive agent is warranted.

Poly-L-lactic acid (PLLA) is a biodegradable polymer with excellent mechanical properties that can be exploited for the formulation of medical devices such as bone screws for bone tissue repair and regeneration [9,10]. However, its hydrophobic nature and degradability into lactic acid-like by-products may lead to inflammation [10]. To overcome

* Corresponding author.
** Corresponding author.
*E-mail addresses:* xmm@dhu.edy.cn (X. Mo), yu.youcheng@zs-hospital.sh.cn (Y. Yu).
[1] These authors contributed equally to this work.

https://doi.org/10.1016/j.compositesb.2022.109920
Received 15 February 2022; Received in revised form 4 April 2022; Accepted 19 April 2022
Available online 26 April 2022

this drawback, blending it with a natural polymer to improve its therapeutic potential has been proposed. Gelatin is a natural polymer with excellent biocompatibility and hydrophilicity. It has been widely used as a suitable candidate for blending with synthetic polymers to expand their medical utilization [11,12]. Hence, we propose blending gelatin with PLLA to fabricate nanofibers (NFs) to yield a composite with improved biocompatibility, rapid degradation, suitable mechanical properties, and hydrophilicity.

Micro- or nanosized fiber structures have shown great potential as scaffolds for bone regeneration and the repair of scar skin tissue defects [13–15]. Among the multiple fabrication methods, electrospinning has emerged as the simplest and most versatile strategy for fabricating NFs for tissue regeneration. The nanosized pores not only facilitate the exchange of gases but also act as a barrier to prevent the migration of fibroblast cells to the defect area [16]. Electrospinning provides multiple options for loading bioactive agents into the polymeric matrix, including homogeneous composites, separated hybrids, and their combinations within all kinds of complicated nanostructures such as core-shell [17–19], and tri-layer core-shell [20]. Among them the coaxial electrospinning and the related core-shell nanofibers are the most popular strategy for encapsulating all types of bioactive agents and ensuring the desired functional performances. Here, electrospun core-shell nanofibers are explored to encapsulate an active ingredient, and the structure-activity relationship for its sustained delivery and GBR application are studied.

Flavonoids derived from plants are a vast group of polyphenolic compounds with antioxidant, anti-cancer, anti-inflammatory, and osteoporotic properties [21]. Epigallocatechin gallate (EGCG) is the most abundant polyphenol present in green tea and is known for its positive effects on bone metabolism [22]. In addition, EGCG has been reported to induce osteogenic differentiation and inhibit adipogenesis, apoptosis, and osteoclastic differentiation of stem cells [23]. Despite its positive effects on bone regeneration, it is difficult to deliver EGCG to the target area in vivo [24]. Oral administration of EGCG reduces its therapeutic efficacy [25]. Sajeesh Kumar et al. coated EGCG on the surface of poly L-lactic acid-based NFs and examined its bone regeneration activity [26]; although the outcomes were promising, the chemical immobilization of EGCG on the surface of NFs can lead to burst release and lower stability [27]. We hypothesized that coaxial electrospinning can be exploited to fabricate a core–shell structure to encapsulate EGCG within the core for better stability and prolonged delivery.

In this study, we fabricated a biodegradable electrospun core–shell NF membrane encapsulated with various concentrations of EGCG. The EGCG-encapsulated membrane exhibited good biocompatibility and antibacterial activity and accelerated bone regeneration.

## 2. Material and methods

### 2.1. Fabrication of NFs

The spinning solutions were prepared by separately dissolving 10% w/v of PLLA (Jinan Daigang Biomaterial, China) and 10% w/v of type A gelatin (Sigma Aldrich) into hexafluoro isopropanol (Aladdin Chemistry, USA) and stirring for 12 h to ensure complete dissolution. The two solutions were mixed at a 60:40 PLLA to gelatin ratio to achieve a 10% w/v final concentration. EGCG was dissolved in phosphate buffered saline (PBS) (Yuanxiang, China) at 5 mg/mL and 10 mg/mL concentrations as a core solution to fabricate PLLA/Gelatin/5 mg/mL EGCG (PG5E) and PLLA/Gelatin/10 mg/mL EGCG (PG10E), respectively.

To fabricate the PLLA/gelatin (PG) fabricate nanofiber membrane, approximately 10 mL of spinning solution was loaded into a syringe with a 21-gauge needle attached to a pump and a power supply. The flow rate was maintained at 1.2 mL/h and the voltage supply was approximately 10 kV. The distance between the collector and the needle was approximately 10 cm. On the other hand, the core–shell NFs were fabricated using a core–shell nozzle connected with two separate pumps. The flow rate for the shell solution was maintained at 1.2 mL/h and that for the core solution was maintained at 0.2 mL/h. A schematic illustration of the core–shell NF fabrication set-up is shown in Fig. 1a. Three types of NFs, PG, PG5E, and PG10E, were fabricated (Fig. 1b).

### 2.2. Membrane characterization

#### 2.2.1. Scanning electron microscopic (SEM) and transmission electron microscopic (TEM) analyses

The surface morphology of the NF membranes was observed using SEM. Dry samples were sputter-coated with gold for 45 s and observed via SEM using Phenom ProX (Phenom, Netherland) at an accelerating voltage of 10 kV. From the SEM images, 100 NFs were randomly selected, measured, and contrasted using ImageJ software (National Institute of Health, USA) to calculate the average NF diameter. To observe the core–shell structure, the samples were prepared by collecting NFs on carbon-coated grids and observed via TEM at a 200-kV accelerating voltage.

#### 2.2.2. Fourier transform infrared (FTIR) detection

To confirm the loading of EGCG and assess the physicochemical interactions of the various components within the NF membranes, FTIR spectra of pure EGCG, gelatin, PLLA, and NF membranes, including PG, PG5E, and PG10E, were obtained at a voltage of 32 scans in the range of 500–3500 $cm^{-1}$ at 25 °C.

#### 2.2.3. Mechanical properties

The mechanical properties of PG, PG5E, and PG10E were evaluated using a universal material testing machine (Instron 5567, USA) at an ambient temperature of 20 °C and humidity of approximately 65% [28]. The specimen was cut to a size of 50 mm × 10 mm (n = 5) and tested with a 10 mm/min cross-head speed until breakage. A digital gauge meter was used to calculate the fiber thickness before the test.

#### 2.2.4. Water contact angle test

The water contact angles of PG, PG5E, and PG10E were measured to assess the surface wettability of the membranes. A distilled water (reference liquid) droplet (n = 3) was automatically dropped on the membranes and the droplet image was visualized using an image analyzer for 5 s. The humidity and temperature were kept constant at 30% and 25 °C, respectively [29]. The water contact angle was calculated using the ImageJ software.

#### 2.2.5. Degradation test

The in vitro degradation tests of the various NF membranes (n = 3) were carried out in PBS [30]. Briefly, the specimens were cut in a circle (20-mm diameter), weighed ($W_0$), poured in PBS (5 mL) in 12-well plates, and kept at 37 °C for 4 weeks. The solution was replaced with fresh solution every 2 d in week 1, followed by weekly replacements in the subsequent weeks. At various time points, the specimens were removed from the solutions, rinsed with deionized water, and lyophilized; the final weight ($W_t$) was then calculated. The remaining mass of the NF membranes at the various time points was calculated using the following equation:

$$\text{Remaining mass } (\%) = W_t/W_0 \times 100.$$

#### 2.2.6. EGCG release experiment

Three samples of PG, PG5E, and PG10E were weighed and placed in a 15-mL centrifuge tube and immersed in 4 mL PBS buffer. The centrifugal tubes were then placed in a 37 °C shaker at an oscillation rate of 100 rpm. At a predetermined time point, 4 mL of liquid was suctioned out and 4 mL of fresh PBS buffer was added. The absorbance of the supernatant was measured using an ultraviolet spectrophotometer (Thermo

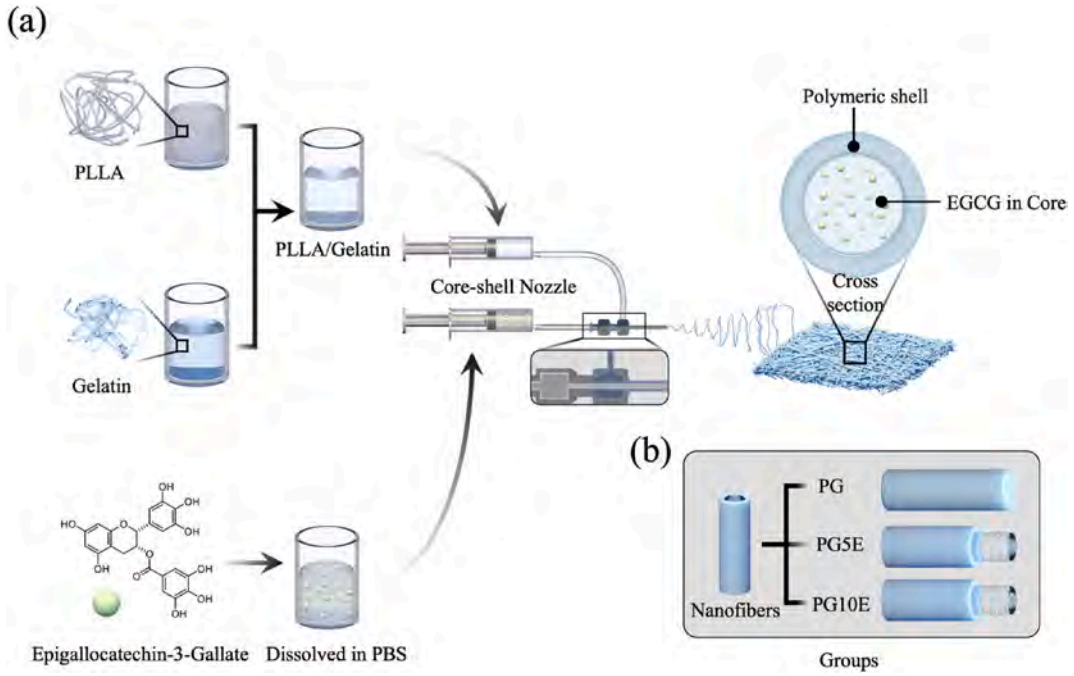


**Fig. 1.** Schematic illustrations. (a) Schematic illustration of the fabrication set-up of the core–shell nanofiber (NF) and (b) the three types of fabricated NFs.

Scientific Evolution 201, USA) at a 206-nm wavelength, and the EGCG concentration was calculated according to the standard curve.

### 2.3. Bone regeneration in vivo

In vivo experiments were conducted following a previously reported procedure [31]. Male white New Zealand rabbits weighing 2500–3000 g, were provided by the Animal Experiment Center of Zhongshan Hospital, Fudan University, maintained at 21–23 °C with full access to standard dry food and water. The animals were assigned to two groups determined by two experimental time points (4 and 8 weeks). The experimental protocol was approved by the Animal Research Committee of Zhongshan Hospital, Fudan University, Shanghai, China (No. 2019–191).

The rabbits were fasted for 4 h before surgery and administered 2% Veto quinol (1 mg/kg body weight) for sedation before administering general anesthesia. Using a 6 mm trephine bur (Nobel, Sweden) and saline irrigation, four symmetrical and circular defects (6-mm diameter) were created in the calvaria of each rabbit. A coin toss was used to assign the faults. Three defects were coated with PG, PG5E, and PG10E, and the fourth defect was left exposed as the control (untreated).

Four or eight weeks after surgery, animals were sacrificed with excessive anesthetics. The harvested samples were scanned using microcomputed tomography (micro-CT) (SKYS-can 1176, Belgium). The software provided by the micro-Ct manufacturer was used for quantitative analyses such as bone mineral density (BMD) and bone volume/tissue volume (BV/TV). Following micro-CT, the samples were decalcified using an Ethylene Diamine Tetraacetic Acid (EDTA) decalcifying solution (Boster AR1071, USA), dehydrated in gradient alcohol, and embedded in paraffin. To visualize tissue healing and bone development, the tissues were sectioned into 5-μm-thick samples and subjected to H&E, Masson and immunohistochemistry (IHC) staining. For IHC, the sections were stained overnight at 4 °C with the primary antibody of ALP (1:100, Abclonal) and OCN (1:100, Abclonal). The secondary antibody against mouse/rabbit IgG were obtained from an IHC kit, EnVision™ Detection Kit (GENE, USA). Diaminobenzidine (DAB) was used for coloration, and the color with dark brown was considered to be the strong positive staining.

Material and methods for biocompatibility, antibacterial activity and osteogenic differentiation in vitro are provided in supplementary information.

### 2.4. Statistical analysis

Data were statistically analyzed using GraphPad Prism software (version 8.0, USA). All quantitative data are expressed as mean ± standard deviation. For continuous variables, data were presented as the means and standard deviations or as medians and interquartile ranges, and groups were compared using analysis of one-way ANOVA or the Kruskal-Wallis test, according to the presence or absence of a normal distribution, respectively. The count data were reported as percentages or ratios, and intergroup comparisons were conducted using the chi-square test. $P < 0.05$ indicated statistical significance. *P*-values for pairwise comparisons between three groups or more were corrected using Bonferroni.

## 3. Results

### 3.1. EGCG encapsulation

The external morphology of the electrospun NFs was characterized via SEM (Fig. 2a–c). All the NF membranes exhibited a web-like randomly oriented fiber structure. No agglomerate or bead formation occurred during the spinning process, confirming the optimum spinning conditions. Based on the average fiber diameter, PG exhibited an average fiber diameter up to 0.85 μm, compared to 0.96 and 0.93 μm for PG5E and PG10E, respectively, indicating that EGCG loading induced a slight increase in the fiber diameter. The core–shell structure that was obtained by loading EGCG into the PG matrix through coaxial electrospinning was confirmed via TEM (Fig. 2d), where a continuous core structure is seen.

FTIR was employed to assess the possible physical or chemical interactions among PLLA, gelatin, and EGCG as well as to confirm the successful EGCG loading through coaxial electrospinning (Fig. 2e). The most prominent representative peak for pure gelatin appeared at 1647 $cm^{-1}$, which can be attributed to C═O stretching in amide 1, highlighted by an orange arrow. The representative peaks for PLLA and gelatin can also be traced in the electrospun PG, PG5E, and PG10E

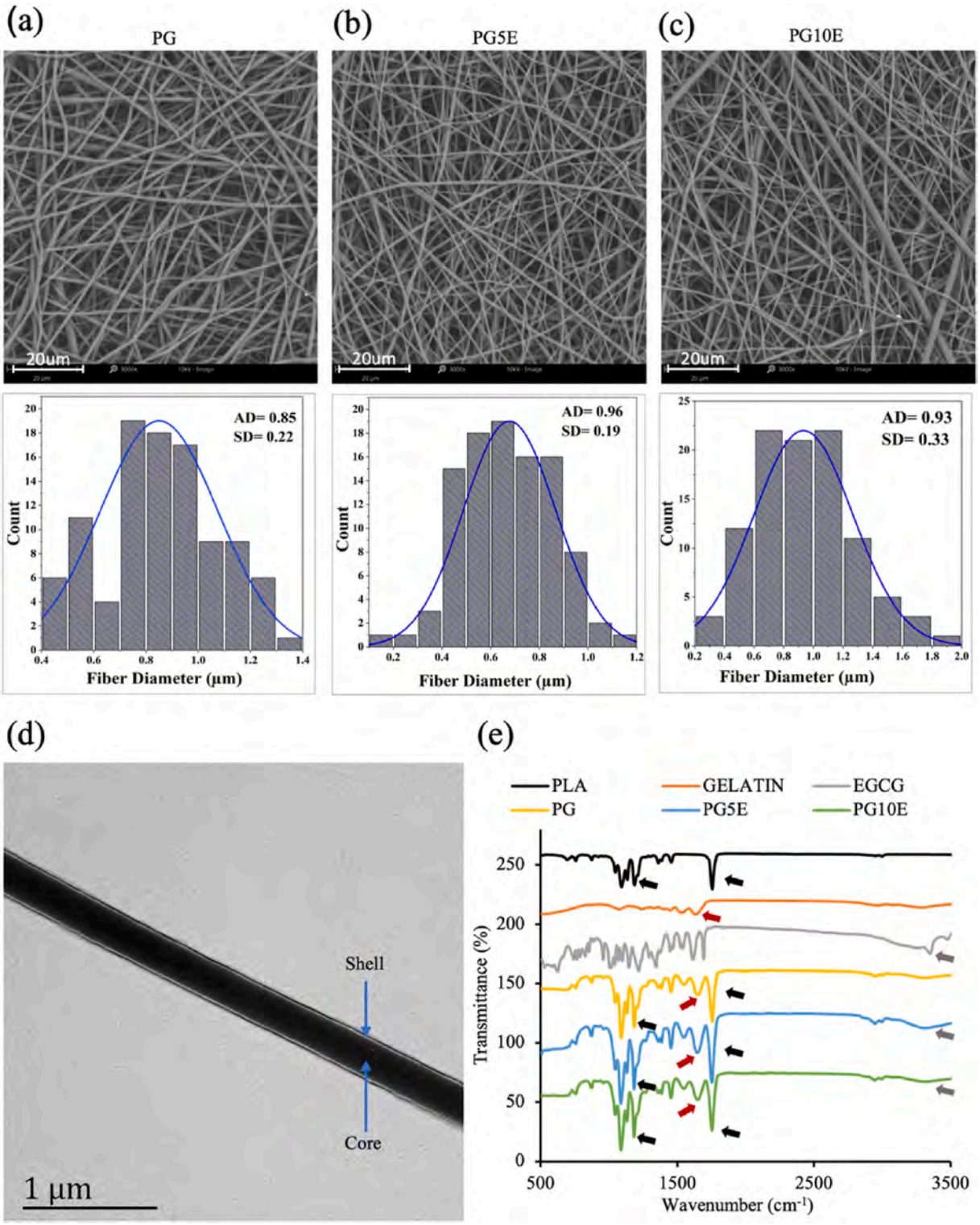


**Fig. 2.** NF membrane morphology. (a–c) Scanning electron microscopy images of the membranes. (d) Transmission electron microscopy image of the membrane with EGCG insertion. (e) Fourier transform infrared spectra of poly-L-lactic acid, gelatin, EGCG, and the PG, PG5E, and PG10E membranes.

spectra, confirming the successful blending of PLLA and gelatin, as highlighted by the respective colored arrows. Multiple peaks appeared for pure EGCG, but a more distinctive peak appeared in the 3200–3500 $cm^{-1}$ range, which can be attributed to the presence of the eight hydroxyl groups. A small peak also appeared in the composite membranes, such as PG5E and PG10E, in the 3200–3500 $cm^{-1}$ range, confirming the presence of EGCG.

### *3.2. Mechanical properties, hydrophilicity, and EGCG sustained-release ability*

A typical stress-strain curve indicated that PG exhibited some obvious elasticity along with tensile strength. With EGCG addition, the PG elastic nature decreased (Fig. 3a). The ultimate PG5E tensile strength was higher than that of PG and PG10E (Fig. 3b). However, the strain

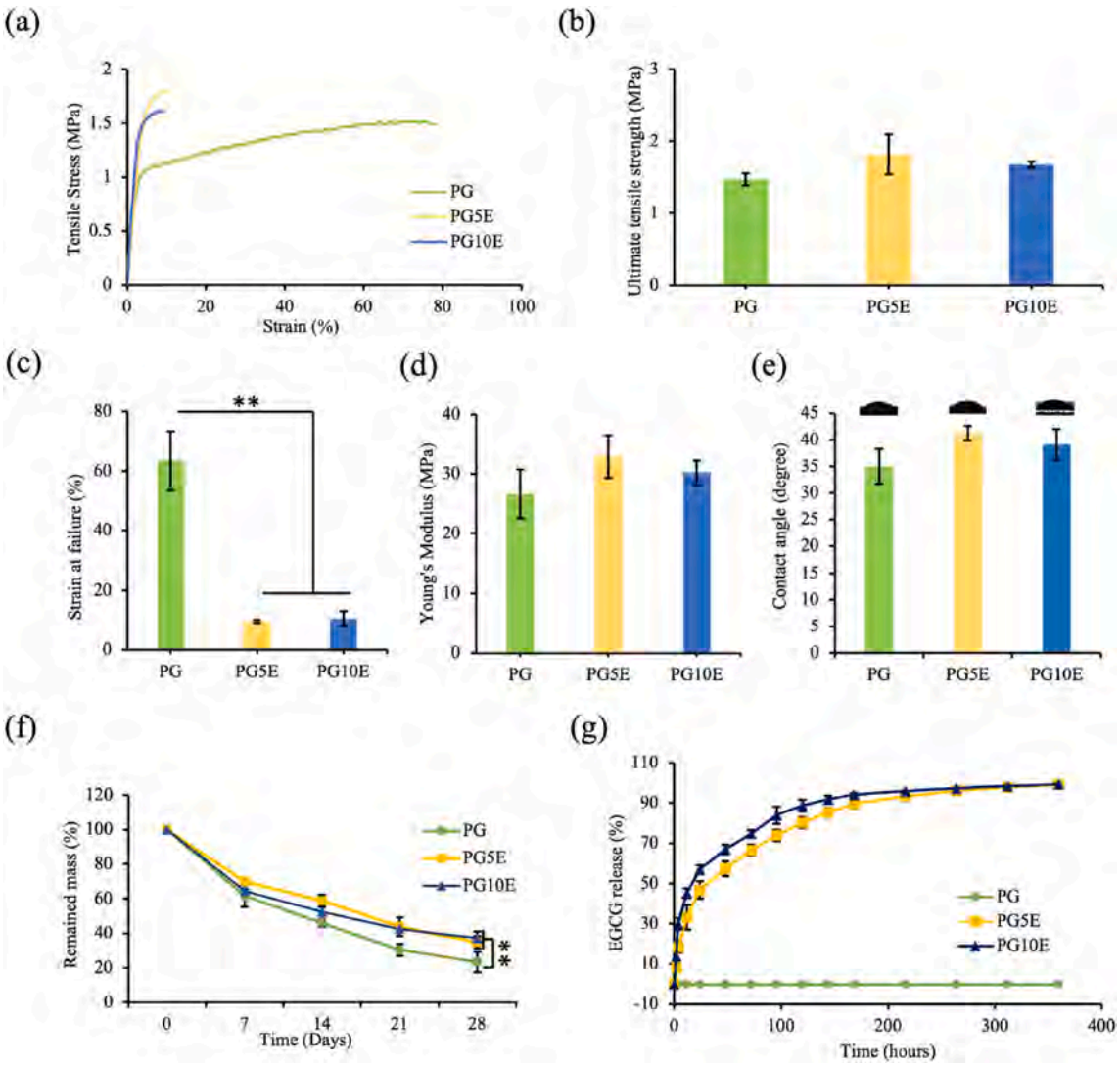


**Fig. 3.** NF membrane characteristics. Representative curves of (a) tensile stress-strain, (b) ultimate tensile strength, (c) strain at failure, and (d) Young's modulus. (e) Water contact angles and (f) degradation profiles in PBS, and (g) cumulative release percentage of EGCG from the membranes in PBS. Statistical analysis was performed by one-way ANOVA followed by Tukey's multiple comparison test, $^{*}P < 0.05$; $^{**}P < 0.01$.

remained significantly low ($P < 0.01$) for both PG5E and PG10E, indicating that EGCG addition and coaxial spinning had an obvious impact on NF elasticity (Fig. 3c). All the NF membranes had a Young's modulus of approximately 30 MPa, with insignificant differences (Fig. 3d).

Surface wettability analyses indicated that all NF membranes were hydrophilic, with a contact angle below 45° (Fig. 3e). Although a slight change in the contact angle was noted among all the membranes, it was statistically insignificant. Overall, EGCG addition did not affect membrane wettability.

The membrane degradation rate in PBS after 28 d (Fig. 3f) was the highest for PG, with a mass loss of approximately 77% ($P < 0.01$), as compared to approximately 65% for PG5E and PG10E.

The EGCG release from PG5E and PG10E was examined by UV spectrometry (Fig. 3g). An initial burst release was observed within the first 72 h. The burst release was more apparent for PG10E, with approximately 70% of the drug being released in the first 72 h. Subsequently, the release rate declined for both membranes, and approximately 90% of drug release was noted during the 168 h assessment. This was followed by the initiation of the sustained release phase, which continued for 360 h, with an estimated total drug release of approximately 99%. In conclusion, three phases of drug release were observed.

### 3.3. Cytotoxicity

The morphology of the co-cultured MC3T3-E1 cells was analyzed by phallacidin and 4',6-diamidino-2-phenylindole (DAPI) staining (Fig. 4a); the cell had a normal shape, with a well-established cytoskeletal network. Moreover, the blue-stained round nuclei confirmed normal cell growth. Cell viability was further confirmed by live-dead staining (Fig. S1a); we could trace an enormous number of uniformly grown viable cells (green) but very few dead cells [32]. The adhesion of the MC3T3-E1 cells to the membrane surface was confirmed using SEM (Fig. 4b) on the third day, where the cells appear to form a dense tissue-like structure. Furthermore, it was concluded that the fabricated membranes were not cytotoxic, based on the cell viability analysis via the Cell Counting Kit-8 (CCK-8) assay (Fig. 4c).

### 3.4. Osteogenesis-inducing capacity in vitro

Alkaline phosphate (ALP) activity acts as a biomarker for early-stage osteogenic differentiation. According to ALP staining on day 14 (Fig. 5a), a more intense purple color on the membranes was observed in the order PG < PG5E < PG10E. Similarly, a darker red color could be traced, in the same order, following Alizarin Red S (ARS) staining

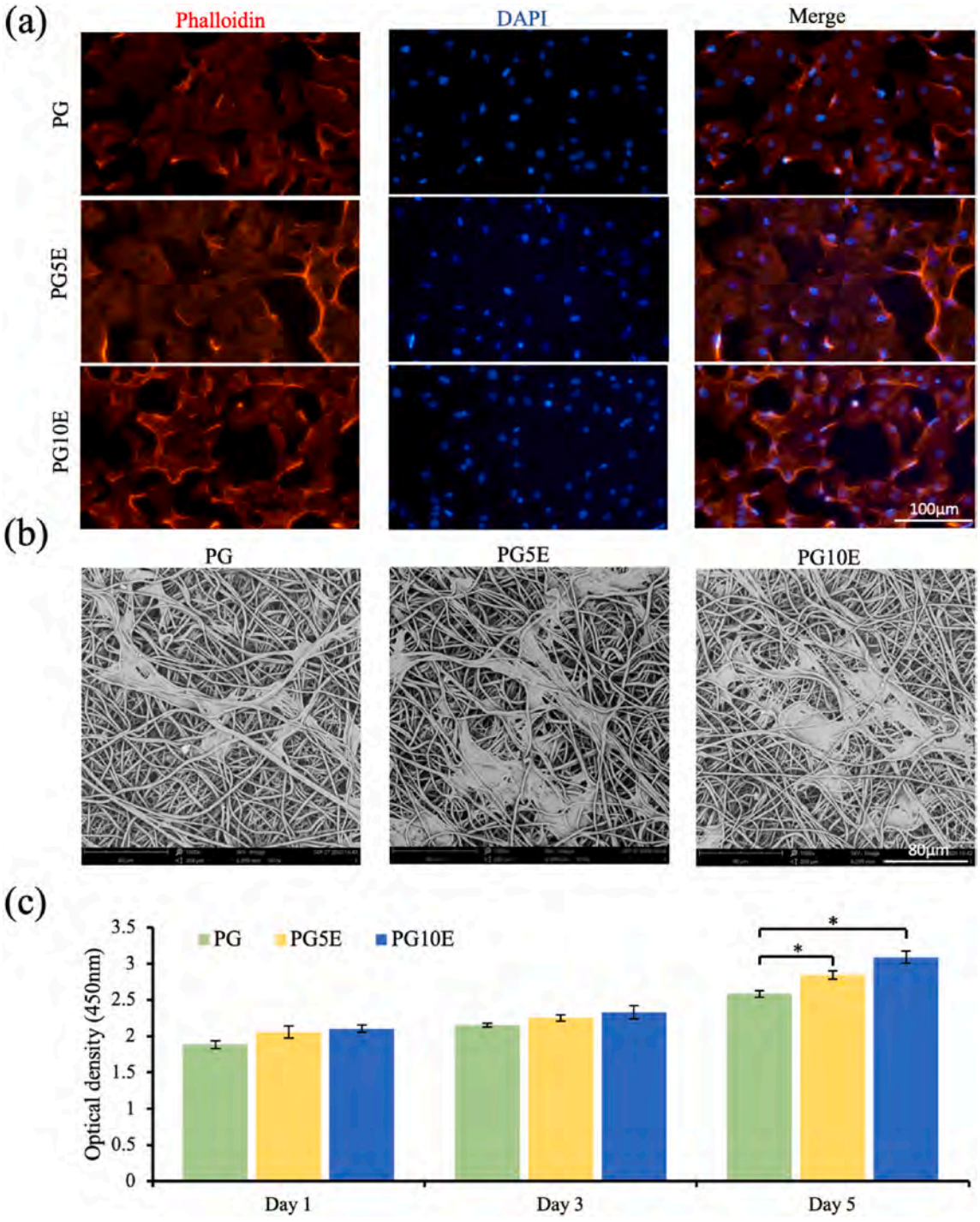


**Fig. 4.** Membrane cytocompatibility evaluation. (a) Phalloidin/DAPI staining, (b) cell morphology results observed via scanning electron microscopy on day 3; (c) MC3T3-E1 cell proliferation on the membranes was measured using the CCK-8 assay. Statistical analysis was performed by one-way ANOVA followed by Tukey's multiple comparison test, $^{*}P < 0.05$; $^{**}P < 0.01$.

(Fig. 5a). Increased calcium deposition, indicated by dark red nodules, was observed on the various membranes. The quantitative analysis was also in line with the qualitative observations. The ALP activity was significantly different and increased in the same order as mentioned above (Fig. 5b). We also noted a significant difference in the mineral content among the various membranes (Fig. 5c). Both activities increased with increasing EGCG concentration.

### 3.5. Antibacterial activity

Microbial infection poses a serious hindrance to periodontal treatment owing to the complex oral environment. The broad-spectrum antibacterial potential of the EGCG-loaded membranes was assessed against *Escherichia coli* (*E. coli)* (Fig. 6a) and *S. aureus* (Fig. 6b) using the colony count method (Fig. 6c–d). Both PG5E- and PG10E-treated groups had fewer visible *E. coli* (Fig. 6a) and *S. aureus* (Fig. 6b) colonies than the PG group. Moreover, a strong correlation was observed between the number of colonies and the EGCG concentration.

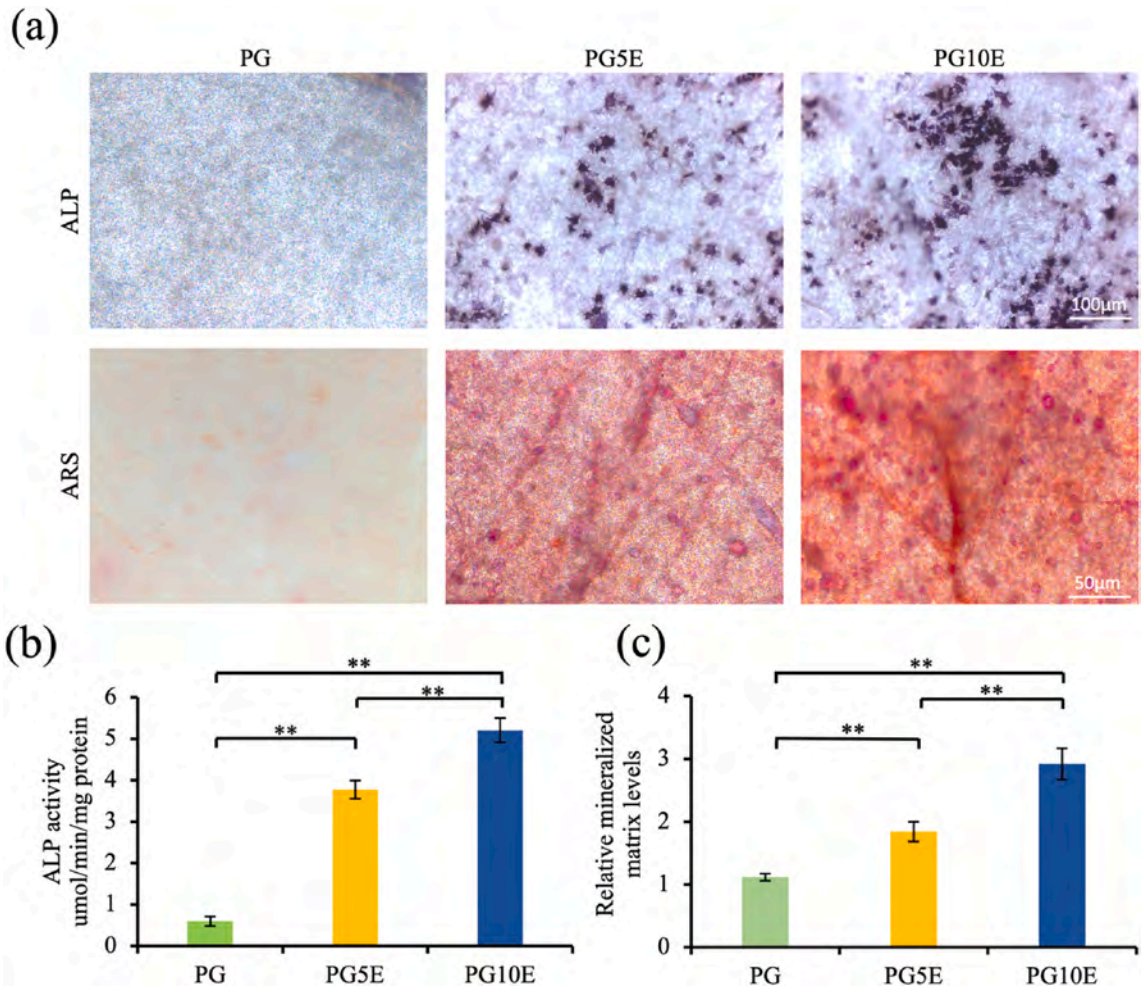


**Fig. 5.** Membranes osteogenesis-inducing capacity. (a) Representative ALP staining and ARS staining on day 14, and determination of (b) ALP activity of MC3T3-E1 and (c) calcium deposition on the membranes. Statistical analysis was performed by one-way ANOVA followed by Tukey's multiple comparison test, $^{*}P < 0.05$; $^{**}P < 0.01$.

### 3.6. Bone regeneration capacity in vivo

We evaluated the PG, PG5E, and PG10E NF membranes for their bone defect recovery and guided bone regeneration potential. Four cranial bone defects were created (Fig. S2a), and three out of four defects were covered by the NF membrane, whereas one remained uncovered (control) (Fig. S2b). The 3D reconstructed micro-CT images were created at weeks 4 (Fig. 7a) and 8 (Fig. 7b) to show the defect recovery progression.

The PG5E- and PG10E-treated groups exhibited considerable progress after week 4. New bone formed from all sides to the center. The PG10E-treated group presented the highest bone formation levels. After week 8, clearer evidence of the healing activity of the various NF membranes was observed. A clear defect was still visible in the control group, whereas the PG-treated group showed a reduction in the defect. A slight defect was observed in the PG5E-treated group; in the PG10E-treated group, better recovery was noted.

Further quantitative analysis of the newly formed bone based on BMD (Fig. 7c) and Bone Volume/Tissue Volume (BV/TV) (Fig. 7d) was conducted. BMD progressed in each group over time, while there was no significant difference in BMD between the control and PG groups at weeks 4 and 8. The BMD level was significantly different ($P < 0.05$) between the PG5E- and PG10E-treated groups at week 4 and also differed from that of the control and PG groups. Therefore, the BMD level is EGCG concentration-dependent. A similar pattern was observed at week 8. The BV/TV quantification results revealed that after weeks 4 and 8, BV/TV levels in the control and NF membrane-treated groups in both weeks were significantly different in the order: control < PG < PG5E < PG10E. These results also imply that the change in BV/TV levels is EGCG concentration-dependent.

We further evaluated the bone defect regenerative activity by sacrificing the rabbits at weeks 4 and 8, followed by H&E and Masson's trichrome staining (Fig. 8a). The surgical margins squeezed the inner ward in the order: control < PG < PG5E < PG10E; this was in line with the observations from the 3D micro-CT reconstructed images. Further evaluation at week 4 showed a void cavity in the defect area filled with some bone marrow and bone cells in both the control and PG-treated groups.

Masson's and H&E staining performed at week 8 further revealed that both EGCG-loaded membranes successfully mediated bone regeneration. Moreover, the regenerative activity happened from the margin to the center in both the PG5E- and PG10E-treated groups (Fig. 8a), whereas the control and PG-treated groups could not form enough bone tissue even after week 8. Masson's staining also indicated that the new bone area (%) in the bone defect measured at 4 weeks (Fig. 8b) was not significantly different for the control and PG groups, with only a slight improvement in the PG-treated group. Comparatively, approximately 40% and 49% of defect areas were covered in the PG5E- and PG10E-treated groups. After 8 weeks (Fig. 8c), the total bone area covered by the control group remained at 42%, compared to 52% in the PG-treated group, while PG5E and PG10E could cover a total of 68% and 78%, respectively. These estimates indicate that new bone formation was

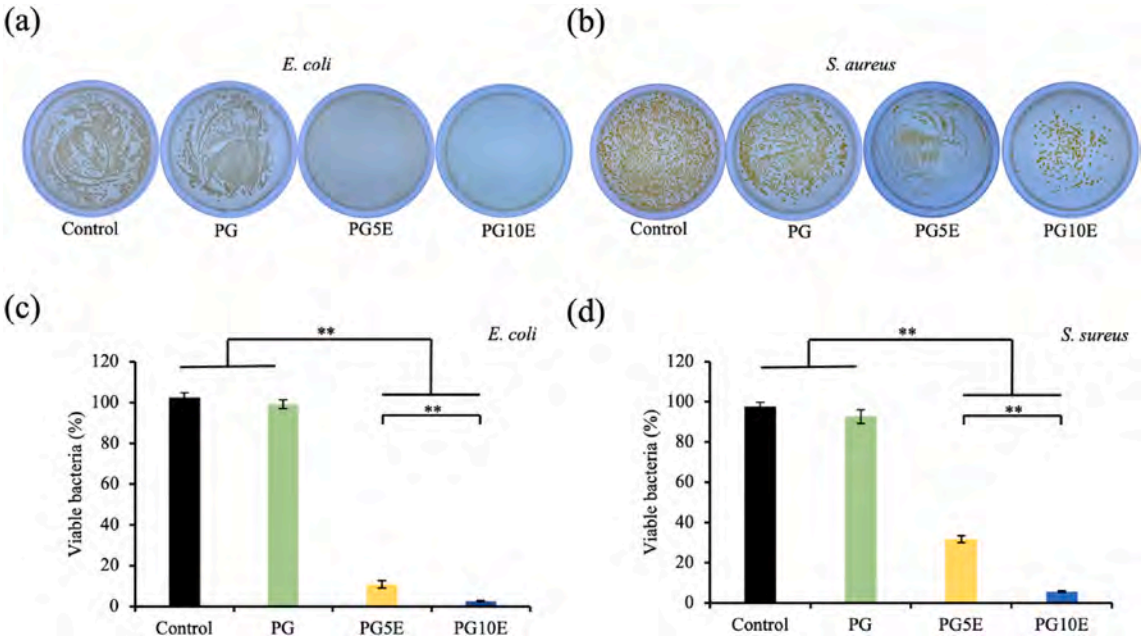


**Fig. 6.** Membrane antibacterial capacity against *E. coli* and *S. aureus*. Digital pictures of agar plates with (a) *E. coli* and (b) *S. aureus* colony-forming units. (c, d) Quantitative bacterial survival rate calculated from the corresponding colony-forming units. Statistical analysis was performed by one-way ANOVA followed by Tukey's multiple comparison test, $^{*}P < 0.05$; $^{**}P < 0.01$.

highly influenced by EGCG content within the NF membranes, in addition to the general benefits of the electrospun NF membrane in regenerative activity.

We selected ALP and Osteocalcin (OCN) as markers for immunohistochemical staining of the sections. At four and eight weeks after surgery, according to the intensity and area of the positive signal, the expression of ALP and OCN in PG10E group was the most obvious, followed by PG5E group, PG group and control group (Fig. S3).

## 4. Discussion

Electrospinning has been broadly demonstrated to be a useful method for encapsulating unstable compounds, and coaxial electrospinning has showed it superiority other processes in term of facile preparation, long-term sustained release, and stability [33–36]. This is particularly advantageous considering the time required for bone regeneration. Thus, we fabricated core–shell membranes with EGCG as the core and PLLA-gelatin NF membranes as the shell.

EGCG could be successfully incorporated into the core without affecting NF surface morphology. Both PG and EGCG-loaded NF membranes showed a smooth surface and continuous fiber structure and no bead formation. This shows that the polymer selection was suitable for our purpose. Smooth and bead-free fiber structures are important for sustained drug release, as beads may interrupt the release process.

Sufficient mechanical strength is a periodontal membrane prerequisite for clinical applicability [36,37]. Appropriate mechanical properties enable the periodontal membrane to maintain its structural integrity during the surgical process and withstand the pressure exerted by newly formed tissues and routine oral activities [38]. The EGCG incorporation within the NF core slightly increased the tensile strength but drastically reduced the strain at failure. However, the impact on Young's modulus remained statistically insignificant. The slight increase in mechanical strength can be correlated to the coaxial fiber structure in which EGCG within the core acted as a reinforcer for the polymeric matrix. The coaxial PLLA/gelatin-based NF mechanical strength superiority is in agreement with a previous report [39]. However, the drastic decrease in the strain at failure indicates that EGCG addition decreased polymer ductility.

Biodegradability is a critical factor in determining regenerative scaffold effectiveness [40,41]. The biodegradation period coordinated with an approximate regenerative time of relevant tissue enhances scaffold clinical applicability. A scaffold that aims to regenerate bone tissue is expected to function between 4 and 6 weeks post-implantation [42]. A fast degradation rate may lead to the membrane structural integrity collapse, whereas very slow degradation may cause failed or inferior regeneration. Despite the excellent PLLA mechanical properties, its biodegradability is slow and incompatible with bone regeneration [43,44]. Gelatine is selected to functionalize PLLA, as it can improve the degradation behavior, the hydrophilicity, and the flexibility [45]. Zhao et al. carried out in vitro degradation of pure PLLA in PBS, found about 4% weight loss in 28 days [46]. Here, all the NF membranes exhibited a mass loss in the 40–50% range after 4 weeks. We also noted an impact of EGCG incorporation and coaxial spinning on the degradation rate, which was statistically significant compared to the impact of neat PG.

We selected coaxial electrospinning to load EGCG within the NF core and demonstrated an around 70% EGCG release within the first 72 h. This rate was better than that reported in a previous study, in which EGCG-loaded liposomes were immobilized on the NF membrane surface, with EGCG released in the same proportion in the first 24 h [47]. The EGCG release can be divided into three distinct phases, which are induced by fiber degradation over time. In phase 1, burst release was predominant owing to the diffusion effect. Because of the NF membrane hydrophilicity, the entry of water prompted the opening of the channels, facilitating EGCG diffusion into the release media. Subsequently, a steady rate was witnessed, followed by a sustained release. These results indicate that coaxial electrospinning facilitates EGCG release with new bone regeneration. Additionally, the initial burst release was significant in balancing the reactive oxygen species level and minimizing bacterial invasion due to the initial inflammatory phase.

A regenerative scaffold must come in direct contact with body tissues, warranting cytotoxicity tests prior to clinical use. Generally, PLLA is considered biologically inert owing to the lack of any bio-functional groups; however, adding gelatin improved cytocompatibility [48]and confirmed to be non-toxic, for gelatin has properties similar to natural collagen [49]. Compared with pure PLLA nanofibrous scaffold, PLLA/-gelatine nanofibrous scaffold enhanced hydrophilicity and significantly

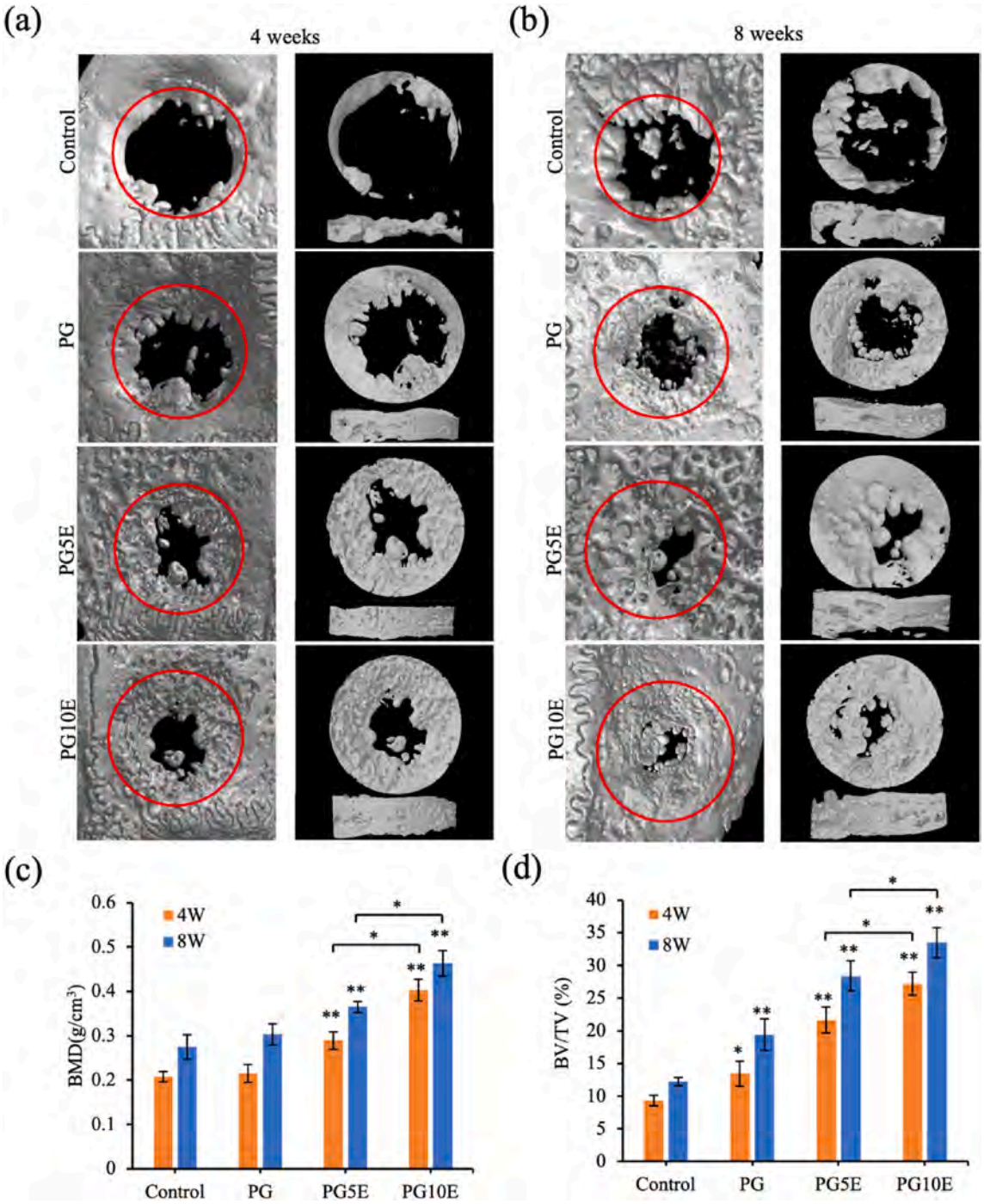


**Fig. 7.** Micro-CT analysis of NF membranes bone repair in vivo. (a–b) Reconstructed three-dimensional micro-CT images at weeks 4 and 8 after EGCG membrane implantation showed the capability of repairing the defect. The bone defect area is indicated by the red circle. Bone tissue parameter analysis of (c) bone mineral density (BMD) and (d) the ratio of bone volume to tissue volume (BV/TV) at weeks 4 and 8. (*$P < 0.05$; **$P < 0.01$, compared to the control group and PG10E compared to PG5E). (For interpretation of the references to color in this figure legend, the reader is referred to the Web version of this article.)

promoted the adhesion, elongation, and proliferation of human chondrocytes [50] bone marrow mesenchymal stem cells [51], epithelial cells and smooth muscle cells [45]. In this study, we observed increased viable cell proliferation on the surface of the EGCG-incorporated membranes. This may be attributed to a more supportive surface for cell adhesion as a result of the presence of many bio-functional groups, such as the favorable interaction of serum proteins with catechol present in the EGCG structure [52]. SEM analysis also confirmed the improved cell adhesion.

In addition to improving cell attachment and proliferation, many studies have confirmed that EGCG or EGCG-incorporated materials have a positive impact on osteogenic activity [23,26,53]. We demonstrated the in vitro osteopromotive activity of the EGCG-based NF membrane by measuring ALP and ARS activity. ALP is a product of osteoblasts and is involved in the breakdown of inorganic pyrophosphate, providing local phosphate and pyrophosphate for bone mineralization [54]. ALP activity can be correlated with osteogenic differentiation. Both ALP and ARS activities were significantly improved by EGCG treatment in a dose-dependent manner.

Although electrospun NFs are advantageous for regenerative activity

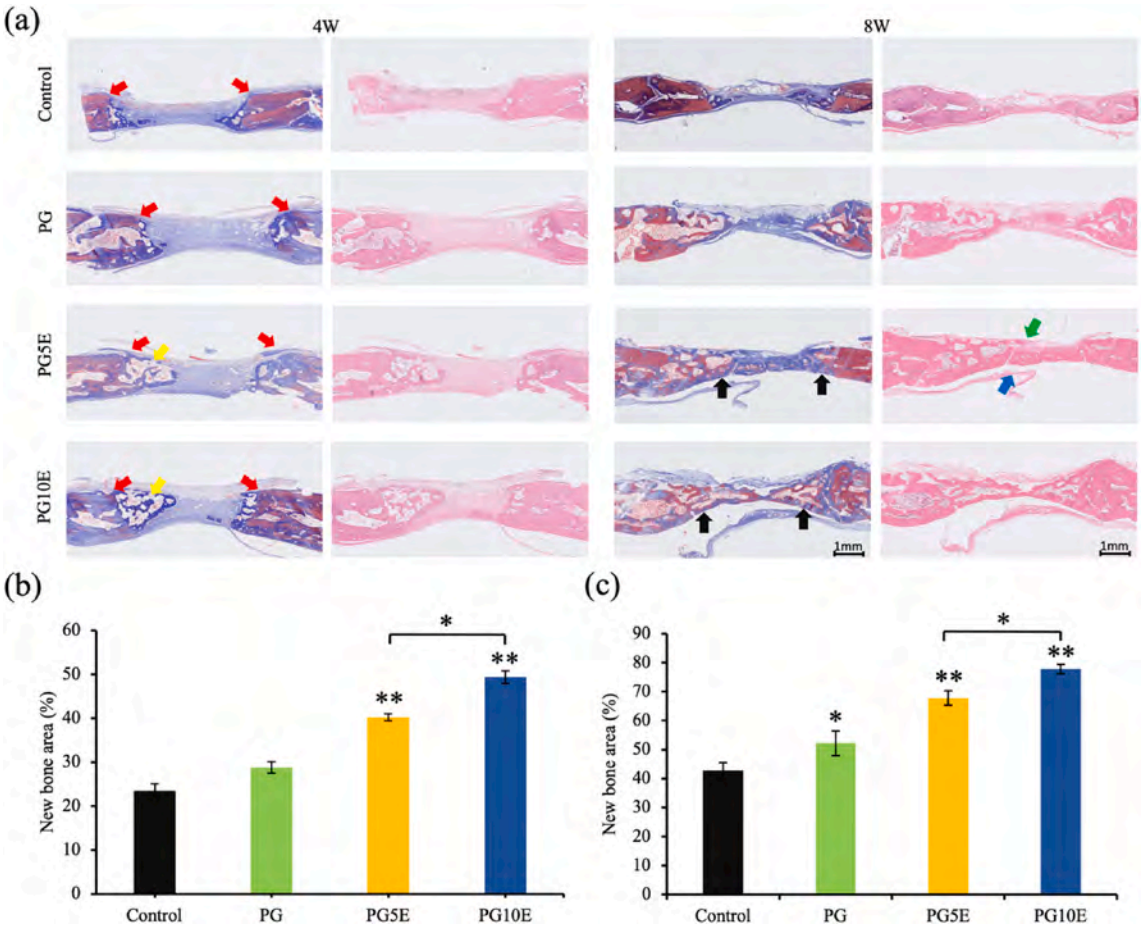


**Fig. 8.** Histological images of newly formed bone tissue. (a) Masson's and H&E staining of decalcified bone tissue at 4 and 8 weeks. (b, c) Analysis of the new bone area at 4 and 8 weeks, respectively. Surgical margins, bone marrow, regenerated bone, periosteal, and endosteal are marked as red, yellow, black, green, and blue arrows, respectively. (*$P < 0.05$; **$P < 0.01$, compared to the control group and PG10E compared to PG5E). (For interpretation of the references to color in this figure legend, the reader is referred to the Web version of this article.)

in multiple ways, biologically inert membranes can increase the risk of bacterial infection due to the surface availability for bacterial attachment, which can further establish biofilm protection from antibacterial drugs [55]. Therefore, a scaffold meant to regenerate body tissues should exhibit antibacterial activity to prevent early-stage infection following membrane implantation [55–57]. The NF membranes containing EGCG were antibacterial and effective against both the gram-negative and gram-positive model strains. Moreover, the antibacterial effect of the membranes increased with increasing EGCG content. The antibacterial activity of EGCG against gram-positive, gram-negative, and multidrug-resistant bacteria had already been established [58–60]. The major mechanism governing the EGCG antibacterial activity is the binding of the negatively charged EGCG with a positively charged bacterial lipid polysaccharide membrane, resulting in reactive oxygen species generation and cell wall destruction [61,62].

Our in vivo bone regeneration studies using a rabbit cranial bone defect model showed that the EGCG-incorporated NF membranes successfully repaired the defects after week 8 in a dose-dependent manner. The reconstructed bone in the PG5E- and PG10E-treated groups almost covered the defect site, although the thickness was lower than that of the pre-defected bone. Without EGCG, the defect area was mostly filled with connective tissue. EGCG and other plant-based polyphenols exhibit osteogenic activities [63,64]. The release of EGCG provided a conducive environment for osteoblast differentiation and progenitor cells. This inhibited fat deposition at the defect site. EGCG also possesses strong antioxidant activity [65], which is highly beneficial in mitigating oxidative stress during the early inflammatory phase of healing. The EGCG bioactivity is highly promising for bone regeneration, and its prolonged and steady localized supply is aided by the electrospun NFs, an ideal delivery platform for EGCG. In addition, hydrophilic NFs are beneficial for absorbing wound exudates and maintaining a clean and conducive environment. Despite the detailed in vitro and in vivo characterization, the exact underlying bone formation mechanisms, especially in vivo anti-inflammatory and antioxidant activities and the related gene expression, remain to be explored.

ALP and OCN are important markers for evaluating new bone formation[66,67]. Therefore, we chose these two markers to evaluate the ability of PG10E, PG5E, PG in promoting new bone formation from protein level. We found that the protein expression levels of ALP and OCN in the EGCG loaded group were significantly higher than those in the EGCG free group at 4 and 8 weeks after surgery, and higher EGCG concentration group had a better bone formation, proving that EGCG loaded degradable fiber membrane has a better effect on promoting bone formation in the defect area.

## 5. Conclusions

In this study, we successfully fabricated a novel multifunctional biodegradable PLLA/gelatin-based NF membrane loaded with EGCG by employing coaxial electrospinning. Extensive physicochemical characterization revealed that the biocompatibility of PLLA can be improved by blending it with gelatin. Moreover, smooth NFs without beads were obtained. EGCG can be loaded within the core of the fiber through coaxial electrospinning without affecting the structure of the NFs.

Moreover, prolonged localized delivery can be achieved. The fabricated membranes were found to be biocompatible and antibacterial and were capable of inducing osteogenic activity, as confirmed through in vitro evaluation. The in vivo trial also revealed that EGCG-incorporated membranes served as bioactive formulations for preventing the migration of fibroblasts into the defect area and aiding in bone regeneration. In conclusion, EGCG is a promising therapeutic agent for bone regeneration and its potential can be magnified by formulating a suitable NF-based delivery platform.

## CRediT authorship contribution statement

**Liang Song:** Methodology, Software, Investigation, Formal analysis, Data curation, and, Writing – original draft. **Xianrui Xie:** Methodology, Investigation, Formal analysis, and, Writing – review & editing. **Cuiting Lv:** Methodology, Investigation, Formal analysis, and, Writing – review & editing. **Atta ur Rehman Khan:** Visualization, Formal analysis, and, Writing – original draft, preparation. **Yang Sun:** Investigation, Resources, and, Visualization. **Ruixue Li:** Investigation, Resources, and, Visualization. **Juan Yao:** Investigation, Resources, and, Visualization. **Mohamed EL-Newehy:** Software, and, Resources. **Hany EL-Hamshary:** Software, and, Resources. **Yosry Morsi:** Software, and, Resources. **Xiumei Mo:** Supervision, Project administration, and, Writing – review & editing. **Youcheng Yu:** Conceptualization, Funding acquisition, Project administrationProject administration, and, Supervision.

## Declaration of competing interest

The authors declare that they have no known competing financial interests or personal relationships that could have appeared to influence the work reported in this paper.

## Acknowledgements

This work was supported by the National Natural Science Foundation of China (82170990, 81870793), Shanghai Science Commission Project (201409006100, 19411950103, 19441902600, 20S31900900, 20DZ2254900, SHDC2020CR5015, SHDC2020CR2042B), Shanghai Municipal Planning Commission of Science and Research Fund (201940382), high-level professional physician training program of Minhang District (2020MZYS08), Scientific Research Project funded by Shanghai Fifth People's Hospital, Fudan University (No. 2020WYZT03), and Sino German Science Foundation Research Exchange Center (M-0263). This project was also supported by Researchers Supporting Project Number (RSP-2021/65), King Saud University, Riyadh, Saudi Arabia, National Advanced Functional Fiber Innovation Center (2021-fx020301), INTERNATIONAL COOPERATION of 2021–2022 China and Poland Science and Technology Personnel Exchange Program (No.17).

## Appendix A. Supplementary data

Supplementary data to this article can be found online at https://doi.org/10.1016/j.compositesb.2022.109920.

## Abbreviations

| | |
|---|---|
| GBR | guided bone regeneration |
| PLLA | poly-L-lactic acid |
| NFs | nanofibers |
| EGCG | epigallocatechin gallate |
| PG | PLLA/gelatin |
| PG5E | PLLA/Gelatin/5 mg/mL EGCG |
| PG10E | PLLA/Gelatin/10 mg/mL EGCG |
| SEM | scanning electron microscopy |
| TEM | transmission electron microscopy |
| FTIR | Fourier transform infrared |
| DAPI | 4′,6-diamidino-2-phenylindole |
| ALP | alkaline phosphatase |
| ARS | alizarin red S |
| micro-CT | microcomputed tomography |
| BMD | bone mineral density |
| BV/TV | bone volume/tissue volume |

## References

[1] Giannoudis PV, Einhorn TA, Marsh D. Fracture healing: the diamond concept. Injury 2007;38(Suppl 4):S3–6.
[2] Uluckan O, Jimenez M, Karbach S, Jeschke A, Grana O, Keller J, et al. Chronic skin inflammation leads to bone loss by IL-17-mediated inhibition of Wnt signaling in osteoblasts. Sci Transl Med 2016;8(330):330ra37.
[3] Yang CY, Yu YR, Wang XC, Wang Q, Shang LR. Cellular fluidic-based vascular networks for tissue engineering. Engineered Regeneration 2021;2:171–4.
[4] Chen Y, Chen L, Wang YT, Lin KL, Liu JQ. Lithium-containing bioactive glasses enhanced 3D-printed PLGA scaffolds for bone regeneration in diabetes. Compos B Eng 2022;230:109550.
[5] Bottino MC, Thomas V, Schmidt G, Vohra YK, Chu TM, Kowolik MJ, et al. Recent advances in the development of GTR/GBR membranes for periodontal regeneration–a materials perspective. Dent Mater 2012;28(7):703–21.
[6] Tsumanuma Y, Iwata T, Washio K, Yoshida T, Yamada A, Takagi R, et al. Comparison of different tissue-derived stem cell sheets for periodontal regeneration in a canine 1-wall defect model. Biomaterials 2011;32(25):5819–25.
[7] Behring J, Junker R, Walboomers XF, Chessnut B, Jansen JA. Toward guided tissue and bone regeneration: morphology, attachment, proliferation, and migration of cells cultured on collagen barrier membranes. Sys. Rev. Odontol. 2008;96(1):1–11.
[8] Rakhmatia YD, Ayukawa Y, Furuhashi A, Koyano K. Current barrier membranes: titanium mesh and other membranes for guided bone regeneration in dental applications. J Prosthodont Res 2013;57(1):3–14.
[9] de Albuquerque TL, Marques Junior JE, de Queiroz LP, Ricardo ADS, Rocha MVP. Polylactic acid production from biotechnological routes: a review. Int J Biol Macromol 2021;186:933–51.
[10] Prabhakaran MP, Venugopal J, Ramakrishna S. Electrospun nanostructured scaffolds for bone tissue engineering. Acta Biomater 2009;5(8):2884–93.
[11] Feng B, Wang S, Hu D, Fu W, Wu J, Hong H, et al. Bioresorbable electrospun gelatin/polycaprolactone nanofibrous membrane as a barrier to prevent cardiac postoperative adhesion. Acta Biomater 2019;83:211–20.
[12] Aldana AA, Abraham GA. Current advances in electrospun gelatin-based scaffolds for tissue engineering applications. Int J Pharm 2017;523(2):441–53.
[13] Li SY, Deng RL, Zou XN, Rong Q, Shou JL, Rao ZL, et al. Development and fabrication of co-axially electrospun biomimetic periosteum with a decellularized periosteal ECM shell/PCL core structure to promote the repair of critical-sized bone defects. Compos B Eng 2022;234:109620.
[14] Ye K, Kuang H, You Z, Morsi Y, Mo X. Electrospun nanofibers for tissue engineering with drug loading and release. Pharmaceutics 2019;11(4):182–98.
[15] Zhang HM, Guo M, Zhu TH, Xiong H, Zhu LM. A careob-like nanofibers with a sustained drug release profile for promoting skin wound repair and inhibiting hypertrophic scar. Compos B Eng 2022;236:109790.
[16] Wu J, Hong Y. Enhancing cell infiltration of electrospun fibrous scaffolds in tissue regeneration. Bioact Mater 2016;1(1):56–64.
[17] Dos Santos DM, Correa DS, Medeiros ES, Oliveira JE, Mattoso LHC. Advances in functional polymer nanofibers: from spinning fabrication techniques to recent biomedical applications. ACS Appl Mater Interfaces 2020;12(41):45673–701.
[18] Liu Y, Chen X, Liu Y, Gao Y, Liu P. Electrospun coaxial fibers to optimize the release of poorly water-soluble drug. Polymers 2022;14(3):469–81.
[19] Li D, Wang M, Song WL, Yu DG, Bligh SWA. Electrospun janus beads-on-A-string structures for different types of controlled release profiles of double drugs. Biomolecules 2021;11(5):635–49.
[20] Wang M, Hou J, Yu DG, Li S, Chen Z. Electrospun tri-layer nanodepots for sustained release of acyclovir. J Alloys Compd 2020;846(12):156471.
[21] Mozaffarian D, Wu JHY. Flavonoids, dairy foods, and cardiovascular and metabolic health: a review of emerging biologic pathways. Circ Res 2018;122(2):369–84.
[22] Nagle DG, Ferreira D, Zhou YD. Epigallocatechin-3-gallate (EGCG): chemical and biomedical perspectives. Phytochemistry 2006;67(17):1849–55.
[23] Lin SY, Kang L, Wang CZ, Huang HH, Cheng TL, Huang HT, et al. (-)-Epigallocatechin-3-Gallate (EGCG) enhances osteogenic differentiation of human bone marrow mesenchymal stem cells. Molecules 2018;23(12):3221–31.
[24] Cai Lj, Xu DY, Chen HX, Wang L, Zhao YJ. Designing bioactive micro-/nanomotors for engineered regeneration. Engineered Regeneration 2021;2:109–15.
[25] Cai ZY, Li XM, Liang JP, Xiang LP, Wang KR, Shi YL, et al. Bioavailability of tea catechins and its improvement. Molecules 2018;23(9):2346–63.
[26] Madhurakkat Perikamana SK, Lee SM, Lee J, Ahmad T, Lee MS, Yang HS, et al. Oxidative epigallocatechin gallate coating on polymeric substrates for bone tissue regeneration. Macromol Biosci 2019;19(4):e1800392.
[27] Huang ST, Hung YA, Yang MJ, Chen IZ, Yuann JP, Liang JY. Effects of epigallocatechin gallate on the stability of epicatechin in a photolytic process. Molecules 2019;24(4):787–99.
[28] Huang K, Jinzhong Z, Zhu T, Morsi Y, Aldalbahi A, El-Newehy M, et al. Exploration of the antibacterial and wound healing potential of a PLGA/silk fibroin based electrospun membrane loaded with zinc oxide nanoparticles. J Mater Chem B 2021;9(5):1452–65.

[29] Huang K, Khalaji MS, Yu F, Xie X, Zhu T, Morsi Y, et al. Multifunctional bioactive core-shell electrospun membrane capable to terminate inflammatory cycle and promote angiogenesis in diabetic wound. Bioact Mater 2021;6(9):2783–800.
[30] Liu X, He X, Jin D, Wu S, Wang H, Yin M, et al. A biodegradable multifunctional nanofibrous membrane for periodontal tissue regeneration. Acta Biomater 2020;108(3):207–22.
[31] Lotfi G, Shokrgozar MA, Mofid R, Abbas FM, Ghanavati F, Baghban AA, et al. Biological evaluation (in vitro and in vivo) of bilayered collagenous coated (nano electrospun and solid wall) chitosan membrane for periodontal guided bone regeneration. Ann Biomed Eng 2016;44(7):2132–44.
[32] Oliveira RR, Fermiano D, Feres M, Figueiredo LC, Teles FR, Soares GM, et al. Levels of candidate periodontal pathogens in subgingival biofilm. J Dent Res 2016;95(6):711–8.
[33] Khan AUR, Huang K, Khalaji MS, Yu F, Xie X, Zhu T, et al. Multifunctional bioactive core-shell electrospun membrane capable to terminate inflammatory cycle and promote angiogenesis in diabetic wound. Bioact Mater 2021;6(9):2783–800.
[34] Jin QH, Fu Y, Zhang GL, Xu L, Jin GZ, Tang LF, et al. Nanofiber electrospinning combined with rotary bioprinting for fabricating small-diameter vessels with endothelium and smooth muscle. Compos B Eng 2022;234:109691.
[35] Yu DG, Wang M, Ge R. Strategies for sustained drug release from electrospun multi-layer nanostructures. Wiley Interdiscip Rev Nanomed Nanobiotechnol; 2021. Dec 28:e1772.
[36] Sasaki JI, Abe GL, Li A, Thongthai P, Tsuboi R, Kohno T, et al. Barrier membranes for tissue regeneration in dentistry. Biomater Investig Dent 2021;8(1):54–63.
[37] Tayebi L, Rasoulianboroujeni M, Moharamzadeh K, Almela TKD, Cui Z, Ye H. 3D-printed membrane for guided tissue regeneration. Mater Sci Eng C Mater Biol Appl 2018;84(3):148–58.
[38] Toledano M, Vallecillo-Rivas M, Osorio MT, Munoz-Soto E, Toledano-Osorio M, Vallecillo C, et al. Zn-containing membranes for guided bone regeneration in dentistry. Polymers 2021;13(11):1797–818.
[39] Kai D, Prabhakaran MP, Stahl B, Eblenkamp M, Wintermantel E, Ramakrishna S. Mechanical properties and in vitro behavior of nanofiber-hydrogel composites for tissue engineering applications. Nanotechnology 2012;23(9):095705.
[40] Gao JJ, Feng L, Chen BL, Fu B, Zhu M. The role of rare earth elements in bone tissue engineering scaffolds - a review. Compos B Eng 2022;235:109758.
[41] Zhu L, Luo D, Liu Y. Effect of the nano/microscale structure of biomaterial scaffolds on bone regeneration. Int J Oral Sci 2020;12(1):6–20.
[42] Sculean A, Nikolidakis D, Schwarz F. Regeneration of periodontal tissues: combinations of barrier membranes and grafting materials - biological foundation and preclinical evidence: a systematic review. J Clin Periodontol 2008;35(8 Suppl):106–16.
[43] Singhvi MS, Zinjarde SS, Gokhale DV. Polylactic acid: synthesis and biomedical applications. J Appl Microbiol 2019;127(6):1612–26.
[44] Bharadwaz A, Jayasuriya AC. Recent trends in the application of widely used natural and synthetic polymer nanocomposites in bone tissue regeneration. Mater Sci Eng C Mater Biol Appl 2020;110(5):110698.
[45] Liu G, Fu M, Li F, Fu W, Zhao Z, Xia H, et al. Tissue-engineered PLLA/gelatine nanofibrous scaffold promoting the phenotypic expression of epithelial and smooth muscle cells for urethral reconstruction. Mater Sci Eng C Mater Biol Appl 2020;111(6):110810.
[46] Zhao Y, Liu B, Bi H, Yang J, Li W, Liang H, et al. The degradation properties of MgO whiskers/PLLA composite in vitro. Int J Mol Sci 2018;19(9):2740–55.
[47] Pires F, Santos JF, Bitoque D, Silva GAj, Marletta A, Nunes VA, et al. Polycaprolactone/gelatin nanofiber membranes containing EGCG-loaded liposomes and their potential use for skin regeneration. ACS Appl Bio Mater 2019;2(11):4790–800.
[48] Lazzeri L, Cascone MG, Danti S, Serino LP, Moscato S, Bernardini N. Gelatine/PLLA sponge-like scaffolds: morphological and biological characterization. J Mater Sci Mater Med 2007;18(7):1399–405.
[49] Asti A, Gioglio L. Natural and synthetic biodegradable polymers: different scaffolds for cell expansion and tissue formation. Int J Artif Organs 2014;37(3):187–205.
[50] Torricelli P, Gioffre M, Fiorani A, Panzavolta S, Gualandi C, Fini M, et al. Co-electrospun gelatin-poly(L-lactic acid) scaffolds: modulation of mechanical properties and chondrocyte response as a function of composition. Mater Sci Eng C Mater Biol Appl 2014;36(3):130–8.
[51] Zhao W, Du Z, Fang J, Fu L, Zhang X, Cai Q, et al. Synthetic/natural blended polymer fibrous meshes composed of polylactide, gelatin and glycosaminoglycan for cartilage repair. J Biomater Sci Polym Ed 2020;31(11):1437–56.
[52] Madhurakkat Perikamana SK, Lee J, Lee YB, Shin YM, Lee EJ, Mikos AG, et al. Materials from mussel-inspired chemistry for cell and tissue engineering applications. Biomacromolecules 2015;16(9):2541–55.
[53] Jin P, Wu H, Xu G, Zheng L, Zhao J. Epigallocatechin-3-gallate (EGCG) as a pro-osteogenic agent to enhance osteogenic differentiation of mesenchymal stem cells from human bone marrow: an in vitro study. Cell Tissue Res 2014;356(2):381–90.
[54] Na K, Kim SW, Sun BK, Woo DG, Yang HN, Chung HM, et al. Osteogenic differentiation of rabbit mesenchymal stem cells in thermo-reversible hydrogel constructs containing hydroxyapatite and bone morphogenic protein-2 (BMP-2). Biomaterials 2007;28(16):2631–7.
[55] Raphel J, Holodniy M, Goodman SB, Heilshorn SC. Multifunctional coatings to simultaneously promote osseointegration and prevent infection of orthopaedic implants. Biomaterials 2016;84(4):301–14.
[56] Lin Z, Zhao Y, Chu PK, Wang L, Pan H, Zheng Y, et al. A functionalized TiO2/Mg2TiO4 nano-layer on biodegradable magnesium implant enables superior bone-implant integration and bacterial disinfection. Biomaterials 2019;219(10):119372.
[57] Xu X, Gu Z, Chen X, Shi C, Liu C, Liu M, et al. An injectable and thermosensitive hydrogel: promoting periodontal regeneration by controlled-release of aspirin and erythropoietin. Acta Biomater 2019;86(3):235–46.
[58] Gordon NC, Wareham DW. Antimicrobial activity of the green tea polyphenol (-)-epigallocatechin-3-gallate (EGCG) against clinical isolates of Stenotrophomonas maltophilia. Int J Antimicrob Agents 2010;36(2):129–31.
[59] Taylor PW, Hamilton-Miller JM, Stapleton PD. Antimicrobial properties of green tea catechins. Food Sci Technol Bull 2005;2:71–81.
[60] Matsumoto Y, Kaihatsu K, Nishino K, Ogawa M, Kato N, Yamaguchi A. Antibacterial and antifungal activities of new acylated derivatives of epigallocatechin gallate. Front Microbiol 2012;3(2):53–62.
[61] Balentine DA, Wiseman SA, Bouwens LC. The chemistry of tea flavonoids. Crit Rev Food Sci Nutr 1997;37(8):693–704.
[62] Chen GP, Zhang H, Wang H, Wang FY. Immune tolerance induced by immune-homeostatic particles. Engineered Regeneration 2021;2:133–6.
[63] Roberto VP, Surget G, Le Lann K, Mira S, Tarasco M, Guerard F, et al. Antioxidant, mineralogenic and osteogenic activities of spartina alterniflora and salicornia fragilis extracts rich in polyphenols. Front Nutr 2021;8(8):719438.
[64] Preethi Soundarya S, Sanjay V, Haritha Menon A, Dhivya S, Selvamurugan N. Effects of flavonoids incorporated biological macromolecules based scaffolds in bone tissue engineering. Int J Biol Macromol 2018;110(4):74–87.
[65] Zhao Z, Feng M, Wan J, Zheng X, Teng C, Xie X, et al. Research progress of epigallocatechin-3-gallate (EGCG) on anti-pathogenic microbes and immune regulation activities. Food Funct 2021;12(20):9607–19.
[66] Brighton CT, Fisher JRS, Levine SE, Corsetti JR, Thibault LE. The biochemical pathway mediating the proliferative response of bone cells to a mechanical stimulus. J Bone Jt Surg Am Vol 1996;78(9):1337–9619.
[67] Li J, Zhang H, Yang C, Li Y, Dai Z. An overview of osteocalcin progress. J Bone Miner Metabol 2016;34(4):367–79.